Journal of Materials Chemistry B

Materials for biology and medicine

www.rsc.org/MaterialsB

Volume 1 | Number 10 | 14 March 2013 | Pages 1373–1510

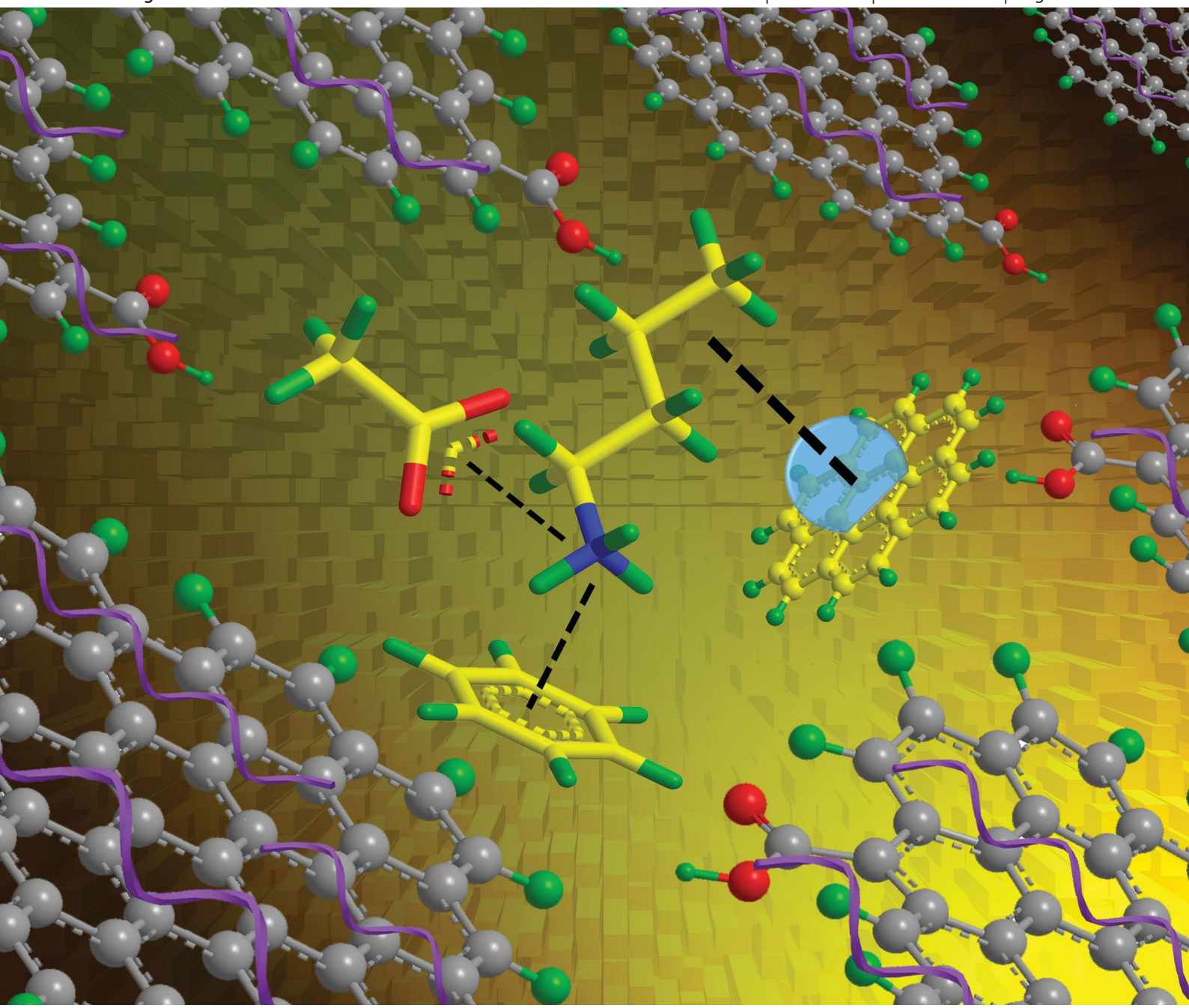

ISSN 2050-750X

RSC Publishing

PAPER

Feng-Bing Wang, Xing-Hua Xia *et al.*

Synthesis of a hydrophilic poly-L-lysine/graphene hybrid through multiple non-covalent interactions for biosensors

2050-750X(2013)1:10;1-1

Journal of Materials Chemistry B

RSC Publishing

PAPER

View Article Online
View Journal | View Issue

Cite this: J. Mater. Chem. B, 2013, 1, 1406

Synthesis of a hydrophilic poly-L-lysine/graphene hybrid through multiple non-covalent interactions for biosensors†

Jiong Wang,[a] Yun Zhao,[a] Fen-Xiang Ma,[a] Kang Wang,[a] Feng-Bing Wang*[ab] and Xing-Hua Xia*[a]

Received 24th November 2012
Accepted 3rd January 2013

DOI: 10.1039/c2tb00454b

www.rsc.org/MaterialsB

Surface modification has been proved to be one of the effective strategies for enhancing the properties of graphene sheets. When a non-covalent modification method is appropriately designed, novel opportunities for better performance of graphene nanosheets can be expected since this strategy can tailor the properties of graphene while its natural structure is retained. This paper introduces a simple route to prepare a highly biocompatible, stable and conductive graphene hybrid modified by poly-L-lysine (PLL) for biosensors using the non-covalent strategy. Results show that PLL adopts a random conformation with the nonpolar parts exposed to outside since its side chains are positively charged under neutral conditions. This conformation allows the strong adhesion of PLL to graphene surface *via* the hydrophobic interaction between butyl chains of PLL and graphene surface, cation–π interaction of protonated amine groups on PLL with the π electrons in graphene, and electrostatic interaction between the protonated amine groups on PLL and the negatively charged carboxyl groups remaining on graphene. All these interactions make the resultant PLL-G hybrid stable and dispersible in aqueous solutions. The resultant hybrid is then used to construct high performance biosensors. As demonstration, hemoglobin (Hb) carrying negative charges can be easily immobilized on the hybrid *via* electrostatic interactions with the positively charged lysine side chains of PLL modified on graphene surface, forming the Hb@PLL-G bionanocomposite. The immobilized protein retains its native structure and exhibits reversible direct electrochemistry. The Hb@PLL-G based enzymatic electrochemical biosensor shows excellent catalytic activity toward its substrate hydrogen peroxide. Its electrochemical response shows the linear dependence of hydrogen peroxide concentration in a range between 10 μM and 80 μM with a detection limit of 0.1 μM. The apparent Michaelis–Menten constant is calculated as 0.0753 mM, demonstrating the significant catalytic ability of the protein. The present strategy can be extended to modify other carbon materials and the resultant nanocomposites are promising for construction of biosensors, bioelectronics and biofuel cells.

Introduction

Graphene with a unique two-dimensional lamellar structure possesses diverse outstanding properties such as large surface area (2630 m^2 g^{-1}), high intrinsic carrier mobility at room temperature ($\approx 10^5$ cm^2 V^{-1} s^{-1}), and excellent mechanical strength and thermal conductivity compared to graphite.[1–4] These properties make graphene an ideal building block for optoelectronics,[5] electronics,[6] supercapacitors,[7–9] fuel cells,[10–14] batteries,[15] photocatalysis,[16,17] photovoltaics,[18] and chemical and biosensors.[19–26] However, a challenge appears since graphene sheets readily stack into graphite in aqueous or most organic media *via* van der Waals and π–π attractions between neighboring sheets.[27] Such irreversible change certainly increases the difficulty of keeping them in storage and degrades the appealing properties of graphene. In addition, it has been reported that intrinsic fullerene and carbon nanotubes are biologically toxic. These nanoscale materials may plug into some proteins or cells *via* the hydrophobic interactions, destroying the biological functions of biomolecules and cells.[28–30] As the basic structural element of some carbon allotropes including graphite, charcoal, carbon nanotubes and fullerenes, intrinsic graphene will be subjected to the same biologically toxic problem when applied to biological systems as

[a]State Key Laboratory of Analytical Chemistry for Life Science, School of Chemistry and Chemical Engineering, Nanjing University, Nanjing 210093, China. E-mail: xhxia@nju.edu.cn; Tel: +86-025-83597436

[b]Nanjing University-Yangzhou Institute of Chemistry and Chemical Engineering, Yangzhou, 211400, China. E-mail: fbwang@nju.edu.cn; Tel: +86-025-83685947

† Electronic supplementary information (ESI) available. See DOI: 10.1039/c2tb00454b

fullerenes and carbon nanotubes. These problems arouse scientists around the world to enhance the properties of graphene through functionalization or by forming hybrids and composites.

As a result, various strategies have been proposed to improve or enhance the surface properties of graphene.[31] Attention is first directed toward covalent modification with chemical bonds of high dissociation energy. This is the most effective method to prevent modifiers detaching from the graphene surface.[32–34] But it also brings the problem that the structural integrity of the sp^2-hybridized carbon network would be interrupted by these new bonds or foreign atoms like nitrogen, boron, sulfur and phosphor. In this regard, non-covalent modification is expected to be a superior strategy. Instead of the covalent modification method *via* strong chemical bond interactions, a non-covalent modification approach through weak or long-range interactions of van der Waals forces, electrostatic forces, coordination bonds and hydrophobic forces, should be easily accessible.[35–42] As it is favorable over these classical interactions, π–π stacking has recently been focused on, since it is relatively strong and will specifically interact with the sp^2-carbon allotropes.[43] For instance, polycyclic aromatic hydrocarbon (PAH) derivatives have been used as typical π-type surfactants for graphene.[44–47] Adsorption of these molecules onto graphene surface is facilitated by the π–π interaction appearing at the aromatic sites. The derivative parts are usually hydrophilic and oriented away from the hydrophobic surface to make the resultant hybrids disperse well in aqueous media.[35,43] Nonetheless, the solubility of PAH derivatives is relatively low in neutral aqueous solutions. It has been reported that the dispersion efficiency is directly related to the surrounding effects, especially the concentration of the modifiers.[48] In order to improve the biological properties and aqueous dispersion of graphene, biomolecules such as peptides and DNA have been proposed to be ideal modifiers.[35,49] Recent works[38,50] have demonstrated that single-stranded DNA (ss-DNA) could easily interact with graphene or CNT to form biocompatible hybrid and increased the solubility in water with potential application in biosensing. With consecutive base pairs serve as the π–π interaction sites, ss-DNA with high solubility is believed to be a better dispersing agent. But for chemically converted graphene, ss-DNA might be an inappropriate modifier since they both carry negative charge which results in electrostatic repulsion to decrease the stability of surface modification. There are reports proving that ss-DNA-graphene hybrid will be decomposed under DNA hybridization with multiple hydrogen bonds.[51,52] These results clearly demonstrate that although non-covalent mode is a powerful approach to improve the properties of graphene, the resultant hybrids or composites may be degraded under inappropriate conditions since single non-covalent interaction is relatively weak.

Poly-L-lysine (PLL) is a polycationic homopolymer of the naturally occurring peptide L-lysine. It is antimicrobial and usually used for cell growth, showing a perfect platform substrate for protecting biomolecules.[53,54] Periodically arranged amine groups make this macromolecule completely soluble in a wide range of solution pH. It has been successfully assembled on graphene using a covalent approach.[55] In this method, high temperature and a large amount of alkali are necessary to complete the ring-opening reaction. Under such critical conditions, the stability of PLL is doubtful as amino linkers may be easily disrupted. Lee and coworkers recently reported the successful preparation of PLL and graphene derivative composite *via* the electrostatic interactions and covalent bonding.[56] The resulted hybrid exhibits high biocompatibility with human cell culture.

Herein, a simple approach to the assembly of PLL on graphene sheets *via* a non-covalent method at room temperature has been proposed to form stable and biocompatible hybrid (PLL-G) in aqueous solutions. The morphology and structures of the PLL-G hybrid were characterized by using electron microscopy, atomic force microscopy and X-ray diffraction microscopy. After the conformation of the assembled PLL on graphene was characterized using circular dichroism spectroscopy, the possible interactions between PLL and graphene have been analyzed in details by the results from zeta potential measurements, Raman and UV-vis spectroscopic characterizations. It is found that PLL adopts random conformation with the nonpolar parts exposed to outside since its side chains are positively charged under neutral conditions, allowing the strong adhesion of PLL to graphene surface *via* hydrophobic interaction, cation–π interaction and electrostatic interaction. Thus, the resultant PLL-G hybrid is stable in aqueous solutions and biocompatible. The potential application of the hybrid in biosensors has been demonstrated. The results demonstrate that the PLL-G hybrid is a promising building block for the construction of biosensors, biofuel cells, bioelectronics and other applications in electrochemical and biological areas.

Experimental section

Reagents

Hemoglobin (Hb, $M_w \sim 64\,500$ from bovine blood), poly-L-lysine hydrobromide (PLL, M_w 30 000–70 000) and Nafion perfluorinated resin solution (5 wt% in mixture of low aliphatic alcohols and water, contains 45% water) were purchased from Sigma (USA). Graphite powder (99.9995%, 100 mesh) was purchased from Alfa Aesar Company (UK). Hydrogen peroxide (H_2O_2, 30% w/w) was purchased from Sinopharm Chemical Reagent Co. Ltd. (Shanghai, China) and its diluted solutions were freshly prepared prior to measurements. Hydrazine solution (A.R.) was purchased from the Nanjing Chemical Reagent Co. Ltd. (Nanjing, China) and used as received. Phosphate buffer solutions (PBS, 20 mM) were prepared by mixing standard stock solutions of K_2HPO_4 and KH_2PO_4. Other reagents were of analytical reagent grade and used as received. All aqueous solutions were prepared with Millipore water with a resistivity of 18.2 MΩ cm.

Apparatus

Zeta potential measurements were performed on a Zetasizer Nano-Z system (USA). The morphology of PLL-G hybrid sample was characterized by transmission electron microscopy (TEM, JEM-200CX, Japan). The TEM samples were prepared by drying

a droplet of the sample suspensions on a Cu grid with carbon film. Images of the surface morphology of the PLL-G modified glassy carbon electrode were taken using a scanning electron microscope (SEM, S-4800, Japan). Thermogravimetric analysis (TGA) and differential scanning calorimetry (DSC) curves were obtained on a STA 449C Jupiter thermoanalyzer (Germany). Atomic force microscope (AFM) images were acquired by using an Agilent 5500 AFM/SPM system with Pico-scan v5.3.3 software. The samples were freshly prepared and dried on a mica plate. Imaging was performed in tapping mode under ambient conditions. X-ray diffraction patterns were obtained on an X-ray powder diffractometer (XRD, X'TRA, Cu K_α radiation, Switzerland) and Raman spectra were recorded on a FT-Raman Spectrometer (Bruker Inc., German). UV-vis spectroscopic characterizations were performed on a UV-3600 Spectrophotometer (optical distance: 10 mm, Shimadzu Scientific Instruments Inc.) or Nanodrop-2000C Spectrophotometer (optical distance: 1 mm, Thermo Fisher Scientific Inc.). Circular dichroism (CD) spectroscopy was carried out on a J-810 Circular Dichroism Spectrometer system (JASCO Corporation, Japan). Electrochemical measurements were performed on a CHI 660D electrochemical workstation (CH Instrument Inc., USA) at room temperature. A conventional three-electrode system was adopted using a saturated calomel electrode (SCE) as the reference, a platinum wire as the counter electrode and the modified glassy carbon electrode as the working electrode. 20 mM, pH 7.0 PBS was chosen as the electrolyte in all experiments.

Preparation of graphene oxide

Graphene oxide (GO) was prepared from graphite according to the Hummers–Offeman method.[57] Briefly, graphite powder (6 g), $K_2S_2O_8$ (3 g) and P_2O_5 (3 g) were mixed in 10 mL concentrated sulfuric acid (18.0 M) and heated to 80 °C for 6 h. The mixture was then diluted and filtered with deionized water. The as-prepared product (2 g) was dispersed in cold concentrated sulfuric acid (18.0 M, 46 mL, dry ice bath), and potassium permanganate ($KMnO_4$, 6 g) gradually added with continuous vigorous stirring and cooling to maintain the temperature below 20 °C. Then, 92 mL deionized water was added into the mixture after heating at 35 °C for 2 h. The reaction was terminated by adding 5 mL H_2O_2 (30%) when the color of the solution turned to bright yellow. The above suspension was then centrifuged and washed with diluted hydrochloric acid. Finally, the suspension was purified by dialysis for a week to remove excess acid and was dried at room temperature to get the solid product.

Preparation of graphene and PLL-G hybrid

To synthesis pure graphene, 10 μL hydrazine hydrates was dropped into 10 mL GO suspension (10 mg GO powder was redispersed in 10 mL water) and refluxed for 1.5 h at 100 °C. The mixture was then rotary evaporated several times to remove excess hydrazine hydrate. After centrifugation, the supernatant of graphene concentration was estimated to be 1.5 mg mL^{-1}. 1 mL graphene dispersion was mixed with 2 mL PLL (2 mg mL^{-1}) and the reaction product was kept static for 12 h at 4 °C to obtain the PLL-G hybrid.

Preparation of Hb-PLL-G/GC electrode

A glassy carbon electrode with a diameter of 3 mm was polished subsequently with 0.3 and 0.05 μm alumina slurries. Then, the electrode was sonicated in ethanol and deionized water prior to use. 5 μL of PLL-G dispersion was cast onto the pretreated GC electrode. A beaker shielded the electrode so that the water could evaporate slowly to form a uniform film on the electrode surface. This modified PLL-G was then used as an excellent matrix for protein immobilization. Immersion of this PLL-G/GC in an Hb solution (3 mg mL^{-1} dissolved in pH = 8.0, 20 mM PBS) for 12 h resulted in immobilization of Hb in the PLL-G matrix, forming an Hb-PLL-G/GC electrode. After that, a protection layer was coated on the modified GC electrode by casting 1 μL of Nafion solution.

Results and discussion

Characterization of the PLL-G hybrid

Graphene suspension (330 μL) was converted from GO through chemical reduction by hydrazine hydrate. The product was diluted to 1 mL. Freshly prepared graphene disperses well in aqueous media, forming a clear suspension without obvious precipitates. If this suspension is kept static for about ten hours, several aggregations occur as shown by Fig. 1a. As we know, the GO suspension is stable because the strong electrostatic repulsion between neighboring GO sheets carrying negative charges formed by deprotonation of surface carboxyl or/and hydroxyl groups. After chemical reduction, most of these oxygen-containing groups will be removed. In reality, a small fraction, especially carboxyl groups at edge section remain, which protect graphene from aggregation temporally.[58,59] Zeta potential measurement shows that the reduced graphene is negatively charged with zeta potential of −9.4 mV (Fig. 1e). The

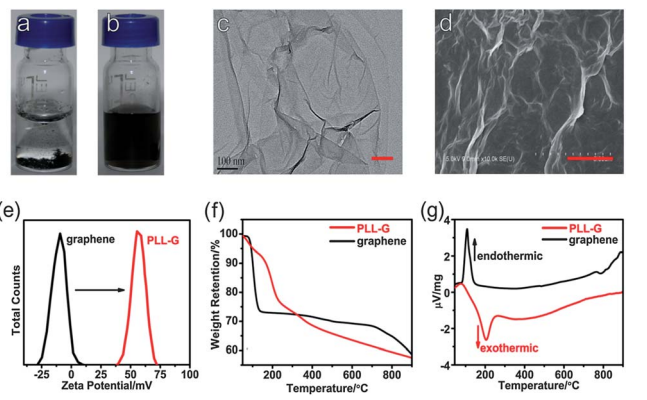

Fig. 1 Digital photos of graphene suspension (0.5 mg mL^{-1}) without (a) and with (b) PLL modification after two weeks. TEM (c) and SEM (d) images of PLL-G. (e) Zeta-potential of chemically reduced graphene in aqueous solution before (black line) and after (red line) PLL modification. TGA (f) and DSC (g) curves of graphene and PLL-G at scan rate of 10 °C per minute in N_2 atmosphere. Scale bar: (c) 100 nm, (d) 3 μm.

absolute value is relatively small, suggesting the instability of a colloidal system.[60] However, the stability of the reduced graphene suspension can be considerably improved if diluted with PLL solution (670 μL). After several months of storage, there are no precipitates observed (Fig. 1b). A TEM image of the PLL-G hybrid reveals an ultra-thin flat sheet with many wrinkled, folded structures and scroll edges (Fig. 1c), showing the typical structure of graphene since perfect two-dimensional atomic crystal is not stable at room temperature. Corrugations unexpectedly make graphene with a large size thermodynamically balanced.[61] When cast on an electrode surface, the wrinkle structures are also observed as indicated by the SEM image (Fig. 1d), demonstrating that PLL-G membrane on the electrode surface also has a similar structure of single layered PLL-G. PLL modification of the reduced graphene results in a change of zeta potential to 57.9 mV (Fig. 1e) which is much larger than the reduced graphene, suggesting more positive surface charges are generated on graphene. The pK_a of PLL is 10.0–10.3.[62] Thus, PLL should be positively charged due to the protonation of amine groups on polymer side chains in nearly neural conditions, which drives the assembly of PLL with negatively charged graphene. Thus, electrostatic interaction between PLL and graphene is one of the driving forces for their assembly.

The electrostatic interaction between PLL and graphene is also confirmed by the TGA and DSC experiments. For the chemically reduced graphene, a weight loss of 26% (Fig. 1f) is observed when the temperature changes from 70 to 140 °C. This can be attributed to the evaporation of residual moisture and pyrolysis of the oxygen-containing groups. The corresponding DSC plot (Fig. 1g) verifies an endothermic peak at around 108 °C, which represents the rate of weight loss reaching a maximum. For the PLL-G hybrid, both the TGA and DSC curves show different features. This hybrid begins to lose weight at a temperature of 50 °C. The corresponding endothermic peak down shifts to 78 °C as well. We assume that the initial weight loss results from strong hygroscopicity of PLL which means that the PLL-G surface carries a certain amount of moisture. In addition, another exothermic peak is observed at around 200 °C, which can be attributed to the crystallization process of polymer chains, proving that PLL has not been disrupted at this temperature.[63,64] Fig. S2† shows that significant weight loss of PLL did not appear until the temperature reached 260 °C. Therefore, it can be concluded that the weight loss of PLL-G hybrid at temperature lower than 200 °C is mainly due to the decomposition of oxygen-containing groups embedded within graphene. Comparing the slopes of the TGA curves for graphene and PLL-G in the temperature range from 50 to 200 °C, it is obvious that the decomposition rate of PLL-G is much slower, suggesting the electrostatic interaction occurs between graphene and PLL.

AFM experiments indicate the average height of freshly prepared graphene nanosheet is about 0.8 nm (Fig. 2a). In contrast, substantial roughness is presented on PLL-G, as well as the average height increases to 2.5 nm (Fig. 2b). The increased thickness of PLL-G should be due to the assembly of PLL at both sides of graphene sheets since the diameter of lysine is 0.863 nm as measured by scanning tunneling

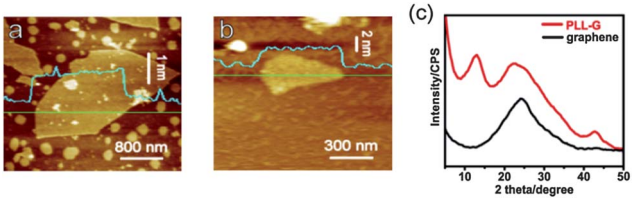

Fig. 2 AFM images and cross-sectional images of graphene (a) and PLL-G (b) on freshly cleaved mica surfaces, and their corresponding X-ray diffraction patterns (c).

microscopy.[65] This result is in good agreement with the one obtained from X-ray diffraction characterizations (Fig. 2c). Pristine graphene shows a characteristic peak at 24.2°, slightly smaller than the 002 reflection of natural graphite as described previously.[66] This discrepancy is expected due to the residual oxygen-containing groups or moisture remaining on graphene sheets. After modification with PLL, the characteristic peak of graphene becomes less sharp. In addition, a new diffraction peak at 12.9° appears, indicating the formation of a new ordered structure. The interlayer distance of PLL-G hybrid, calculated based on the Bragg's equation, is 6.68 Å, approximately representing the average thickness of PLL on graphene, which is in good agreement with the AFM results as well.

Raman spectroscopy is able to distinguish graphene from graphite, and is very sensitive to the surface charge (namely doping effect), structural defects and layer numbers.[67] In this work, the Raman spectra were recorded with a laser excitation wavelength of 514 nm. Both the samples display the typical D-band, G-band and 2-D band of graphene (Fig. 3). The 2-D band at 2678 cm^{-1} is the second harmonic of D-band, which can be used to decide the layer numbers of graphene.[68] As shown in Fig. 3, the 2-D band of PLL-G is more intense and sharper than that of pristine graphene, indicating few layers of graphene in the PLL-G system due to the effective protection effect of PLL. The two well-defined bands between 1350 and 1600 cm^{-1} reflect the structural defects (D-band, 1350 cm^{-1}) and graphitization degree (G-band, 1594 cm^{-1}) of graphene, respectively.[69] The intensity ratio of D-band to G-band (I_D/I_G) increases from 0.91 to 1.09 before and after PLL modification of graphene. In our measurements, PLL does not show any Raman signals within the studied wavenumber range. The stronger

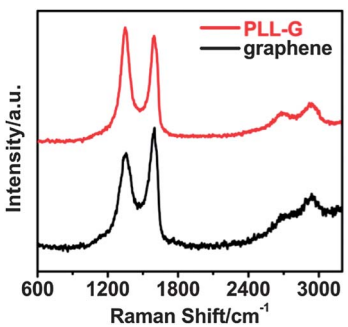

Fig. 3 Raman spectra of graphene and PLL-G.

D-band intensity should be ascribed to the electronic structure of sp^2-carbon atoms on graphene.[70,71] Therefore, the Raman characterizations imply that other driving forces are involved in the assembly of PLL onto the graphene surface besides the electrostatic interaction mentioned above.

The ultraviolet-visible (UV-vis) spectrum reflects the state of valence electrons in graphene. As shown in Fig. 4a, the pristine graphene displays a maximum absorption by π–π* electron transition at 233 nm, attributed to the rich sp^2-carbon atoms. After immobilization of PLL, the formed PLL-G hybrid shows an absorption peak at 266 nm with a significant red shift, indicating that some groups on PLL have conjugated with the π-electrons of graphene. The UV-vis absorption of pure PLL locates at 217 nm. Around this wavelength, only protonated amine groups on polymer side chains with n–π* electron transition or carbonyl groups on polymer backbone with π–π* electron transition is allowed, while the transition probability of the latter is apparently much higher. In the presence of graphene, the absorption of PLL inversely blue shifts to 208 nm, meaning that the carbonyl groups cannot conjugate with graphene. Therefore, only protonated amines are suggested to conjugate with graphene *via* the cation–π interaction as reported previously.[70] It has been reported that cation–π interaction is widely present within biomolecules *via* the interaction between partial inorganic cations and polar organic groups with the aromatic systems. Lee and coworkers[72] recently demonstrated that potassium and sodium ions can be fixed on the surface of graphene by cation–π interaction. The incorporation of cations shifts the Fermi level of graphene to the conduction band, displaying an n-type doping effect. In the present work, once amine is protonated, its binding energy with aromatic rings will be comparable to the one from potassium ions.[71] From both the Raman and UV-vis spectra, we can assume that PLL functions as a doping agent for graphene. The arrangement of π-electrons in PLL modified graphene is altered through electron conjunction, which will change the surface charge of graphene as confirmed by the increase of I_D/I_G ratio (Fig. 3).

We propose that the observed blue shift in the UV-vis spectrum of PLL-G relates to the structural transformation of PLL in the PLL-G hybrid. The secondary structure of PLL is sensitive to external conditions.[73] For instance, at pH 12, strong intra/intermolecular hydrogen bonds are generated on PLL by the deprotonated amines. In Fig. 4d, the circular dichroism (CD) spectrum presents double negative peaks at 210, 222 nm and a positive peak at 196 nm, indicating the rich alpha-helix conformation of PLL. If adjusting the solution pH to 5.9, amine groups will be protonated. Thus, the hydrogen bonds will be replaced by the electrostatic repulsion. In this case, the CD curve displays only one negative peak at 197 nm and one broad positive peak around 217 nm, indicating that the secondary structure of PLL mainly takes the random-coil conformation.[74] This change in conformation can also be observed by the change of UV-vis absorbance band of PLL for pH 5.9 to 12 (Fig. 4c). In the presence of graphene, the intra/intermolecular interaction of PLL is disturbed by the electrostatic and cation–π interactions as mentioned above. The random conformation of PLL transfers to another status as reflected by the CD results (Fig. 4b). In addition, comparing with the ordered α-helix or β-sheets, the random conformation of PLL is more beneficial for exposing its nonpolar parts (butyl chains with relatively hydrophobic properties). Therefore, the hydrophobic force between the butyl chains and the surface of graphene also participates in forming the PLL-G assembly.

Based on the above analysis, the modification mechanism of PLL onto the surface of graphene can be summarized as in Fig. 5. In the PLL-G assembly, PLL adopts a random conformation with the nonpolar parts exposed to the outside since its side chains are positively charged under neutral conditions. This conformation allows the strong adhesion of PLL to the surface of graphene *via* the hydrophobic interaction between the butyl chains of PLL and the surface of graphene, cation–π interaction of protonated amine groups on PLL with the π electrons in graphene, and electrostatic interaction between the protonated amine groups on PLL and the negatively charged carboxyl groups remaining on graphene. All these interactions make the resultant PLL-G hybrid stable and dispersible in aqueous solutions.

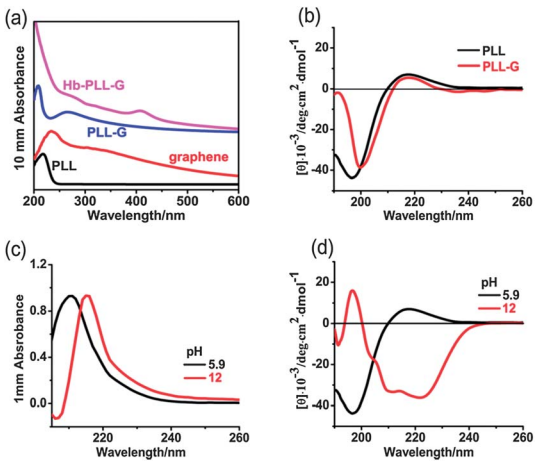

Fig. 4 (a) UV-vis spectra of PLL, graphene, PLL-G and Hb-PLL-G. (b) CD spectra of PLL in aqueous solutions with and without adding graphene. (c) UV-vis spectra of PLL in aqueous solutions with pH values at 5.9 and 12. (d) Corresponding CD spectra of PLL in aqueous solutions with pH values at 5.9 and 12.

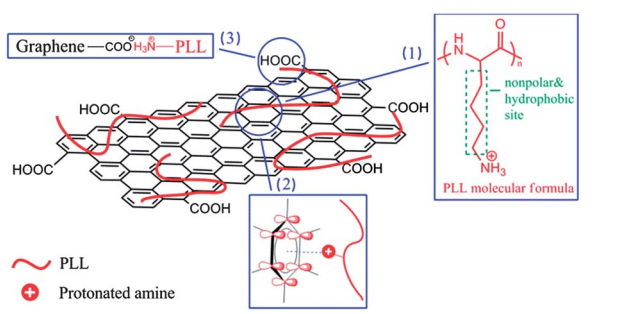

Fig. 5 Schematic representation of the driving forces taking part in the assembly of PLL onto graphene surface, including (1) hydrophobic interaction, (2) protonated amine–π electrons interaction and (3) electrostatic interaction.

Direct electrochemistry of Hb-PLL-G on GC electrode

The immobilized Hb was first characterized using UV-vis spectroscopy. As shown in Fig. 6a, a soret band of the immobilized Hb appears at 409 nm, which is centered at the same wavenumber as that for Hb in solution. This demonstrates the immobilized Hb retains its natural conformation. In addition, the immobilized Hb can exchange electrons directly with the electrode (Fig. 6b). As expected, the pure PLL-G modified electrode does not show any Faradaic features besides the double layer charging. While, the Hb-PLL-G/GC electrode shows a pair of well-defined and quasi-reversible redox peaks with a cathodic peak at −0.388 V (*vs.* SCE) and an anodic peak at −0.327 V (*vs.* SCE). The formal potential $[E^{0'} = 1/2(E_{pc} + E_{pa})]$ is −0.356 V (*vs*. SCE), coinciding with the characteristic heme redox couple of Hb reported previously.[75,76] Fig. 6c and d show that both the anodic and cathodic currents linearly increase with increasing the scan rate, suggesting the process of direct electron transfer is surface-controlled. From the peak-to-peak separations in Fig. 6e, the rate constant (k_s) of direct electron transfer can be determined according to the Laviron's equation.[77] Assuming the charge-transfer coefficient $\alpha = 0.5$ and the number of electrons ($n = 1$) for one electron transfer process, *ks* is calculated to be 5.7 s^{-1}. In addition, it is found that the formal potential ($E^{0'}$) of the redox couple changes linearly with solution pH from 4.47 to 9.26 (Fig. 7a). A slope of about −49.8 mV/pH (Fig. 7b) implies single proton taking part in the electron communication of Hb with the underlying electrode.

Electrocatalytic activity of the Hb-PLL-G/GC electrode toward hydrogen peroxide reduction

The electrocatalytic activity of the Hb-PLL-G/GC electrode toward H_2O_2 was also studied by cyclic voltammetry. As presented by Fig. 8a, upon addition of 2 mM H_2O_2 into the PBS electrolyte, the reduction current became considerably larger, originating from the reduction of H_2O_2 catalyzed by the active center of immobilized Hb. In contrast, the PLL-G/GC electrode shows a much smaller response to the same amount of H_2O_2.

The observed significant electrocatalytic activity of Hb immobilized in the matrix of PLL-G enables us to sensitively detect H_2O_2 in solutions. As shown in Fig. 8b, the amperometric response of Hb-PLL-G/GC electrode keeps increasing with successively injecting 10 μM H_2O_2 into the testing solution. The calibration curve of the current response as a function of H_2O_2 concentration is linear in the concentration ranging from 10 μM to 80 μM (the correlation coefficient of 0.997) with a detection limit of 0.1 μM ($S/N = 3$).

The apparent Michaelis–Menten constant, K_m^{app}, is an important parameter representing the affinity of enzyme to the substrate in the constructed system. The numerical value of K_m^{app} is equal to the concentration of the substrate when the enzymatic reaction speed reaches the half maximum, which can be estimated in terms of the Lineweaver–Burk equation, (1),

$$1/i_{ss} = 1/i_{max} + 1/K_m^{app}C \quad (1)$$

where, i_{ss} is the steady-state current, C is the H_2O_2 concentration, and i_{max} represents the maximum current. The K_m^{app} is calculated to be 0.0753 mM according to eqn (1). This value is much smaller than that obtained in many other papers,[78,79] demonstrating the catalytic ability of Hb is well retained in our system.

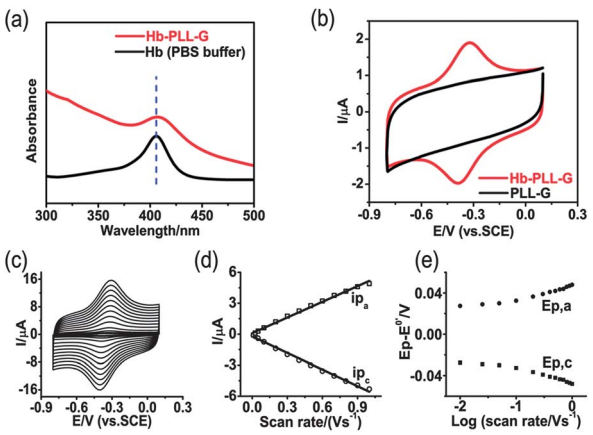

Fig. 6 (a) UV-vis spectra of free Hb in PBS buffer (pH = 7.0) and Hb-PLL-G in pure water. (b) Cyclic voltammograms of the PLL-G/GC and Hb-PLL-G/GC electrodes in a N_2-saturated PBS (20 mM pH = 7.0) at a scan rate of 100 mV s^{-1}. (c) Cyclic voltammograms of the Hb-PLL-G/GC electrode in a N_2-saturated PBS (20 mM pH = 7.0) at different scan rate of 0.01, 0.025, 0.05, 0.1, 0.2, 0.3, 0.4, 0.5, 0.6, 0.7, 0.8, 0.9 and 1.0 V s^{-1}. (d) Plot of the corresponding cathodic and anodic peak currents *versus* scan rate. (e) Plot of the corresponding cathodic and anodic peak potentials *versus* logarithm of scan rate.

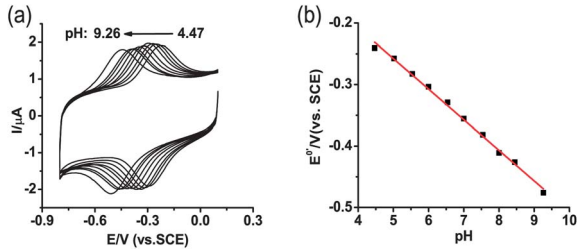

Fig. 7 (a) Cyclic voltammograms of the Hb-PLL-G/GC electrode in a N_2-saturated PBS with different pH values (from right to left) at 4.47, 5.02, 5.54, 6.00, 6.54, 7.00, 7.54, 8.00, 8.45 and 9.26. (b) Plot of the formal potential ($E^{0'}$) *versus* solution pH.

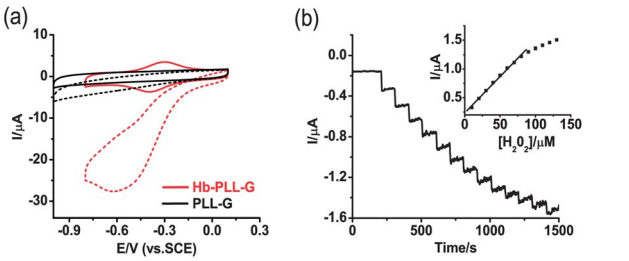

Fig. 8 (a) Cyclic voltammograms of the modified electrodes in PBS (20 mM pH = 7.0, scan rate 100 mV s^{-1}). Hb-PLL-G/GC and PLL-G/GC electrodes in N_2-saturated PBS before (solid curves) and after (dashed curves) adding 2 mM H_2O_2. (b) Current responses of the Hb-PLL-G/GC electrode at −0.35 V (*vs.* SCE) upon successive injecting 10 μM H_2O_2 into 10 mL N_2-saturated PBS (20 mM, pH = 7.0). Inset shows the corresponding calibration plot.

Conclusions

In summary, we have proposed a new strategy to prepare a highly compatible and stable graphene hybrid using PLL and applied this novel hybrid as an excellent matrix to immobilize Hb. As indicated by experimental results, hydrazine hydrate reduced graphene carries weak negative charges and PLL adopts random conformation in neutral solution. The assembly of PLL on graphene surface is droved by multiple non-covalent interactions, including the electrostatic interaction, cation–π interaction, and hydrophobic interaction. Multiple non-covalent interactions preserve the pristine properties of graphene after assembling with PLL, while the stability, dispersibility and biocompatibility have been significantly improved. For example, the immobilized hemoglobin in PLL-G matrix can ready exchange electrons with the underlying electrode and its biocatalytic activity is retained. The present non-covalent approach for synthesis of a PLL-G hybrid with enhanced properties compared to graphene shows various advantages and the resultant hybrid will provide a promising platform for exploring the application of graphene or analogous carbon materials as biomaterials and building blocks for the construction of biosensors, bioelectronics and biofuel cells.

Acknowledgements

This work was supported by grants from the National 973 Basic Research Program (2012CB933800), the National Natural Science Foundation of China (21035002, 21205059), the National Science Fund for Creative Research Groups (21121091), and the Natural Science Foundation of Jiangsu province (BK2010009, BK2011440).

Notes and references

1 A. K. Geim, K. S. Novoselov, S. V. Morozov, D. Jiang, Y. Zhang, S. V. Dubonos, I. V. Grigorieva and A. A. Firsov, *Science*, 2004, **306**, 666–669.
2 S. Park and R. S. Ruoff, *Nat. Nanotechnol.*, 2009, **4**, 217–224.
3 Y. B. Zhang, Y. W. Tan, H. L. Stormer and P. Kim, *Nature*, 2005, **438**, 201–204.
4 A. K. Geim and K. S. Novoselov, *Nat. Mater.*, 2007, **6**, 183–191.
5 Z. P. Sun, T. Hasan, F. Torrisi, D. Popa, G. Privitera, F. Q. Wang, F. Bonaccorso, D. M. Basko and A. C. Ferrari, *ACS Nano*, 2010, **4**, 803–810.
6 Q. He, S. Wu, S. Gao, X. Cao, Z. Yin, H. Li, P. Chen and H. Zhang, *ACS Nano*, 2011, **5**, 5038–5044.
7 Q. Wu, Y. Xu, Z. Yao, A. Liu and G. Shi, *ACS Nano*, 2010, **4**, 1963–1970.
8 X. Cao, Y. Shi, W. Shi, G. Lu, X. Huang, Q. Yan, Q. Zhang and H. Zhang, *Small*, 2011, **7**, 3163–3168.
9 Z. S. Wu, W. C. Ren, D. W. Wang, F. Li, B. L. Liu and H. M. Cheng, *ACS Nano*, 2010, **4**, 5835–5842.
10 L. Qu, Y. Liu, J.-B. Baek and L. Dai, *ACS Nano*, 2010, **4**, 1321–1326.
11 Z.-H. Sheng, L. Shao, J.-J. Chen, W.-J. Bao, F.-B. Wang and X.-H. Xia, *ACS Nano*, 2011, **5**, 4350–4358.
12 Y.-G. Zhou, J.-J. Chen, F.-b. Wang, Z.-H. Sheng and X.-H. Xia, *Chem. Commun.*, 2010, **46**, 5951–5953.
13 Z.-H. Sheng, H.-L. Gao, W.-J. Bao, F.-B. Wang and X.-H. Xia, *J. Mater. Chem.*, 2012, **22**, 390–395.
14 Y. Li, T. Li, M. Yao and S. Liu, *J. Mater. Chem.*, 2012, **22**, 10911–10917.
15 Z.-S. Wu, W. Ren, L. Wen, L. Gao, J. Zhao, Z. Chen, G. Zhou, F. Li and H.-M. Cheng, *ACS Nano*, 2010, **4**, 3187–3194.
16 H. Zhang, X. Lv, Y. Li, Y. Wang and J. Li, *ACS Nano*, 2010, **4**, 380–386.
17 L. Han, P. Wang and S. Dong, *Nanoscale*, 2012, **4**, 5814–5825.
18 N. Yang, J. Zhai, D. Wang, Y. Chen and L. Jiang, *ACS Nano*, 2010, **4**, 887–894.
19 H.-L. Guo, X.-F. Wang, Q.-Y. Qian, F.-B. Wang and X.-H. Xia, *ACS Nano*, 2009, **3**, 2653–2659.
20 B.-Y. Hua, J. Wang, K. Wang, X. Li, X.-J. Zhu and X.-H. Xia, *Chem. Commun.*, 2012, **48**, 2316–2318.
21 Z.-H. Sheng, X.-Q. Zheng, J.-Y. Xu, W.-J. Bao, F.-B. Wang and X.-H. Xia, *Biosens. Bioelectron.*, 2012, **34**, 125–131.
22 Y. Wang, Y. Shao, D. W. Matson, J. Li and Y. Lin, *ACS Nano*, 2010, **4**, 1790–1798.
23 W. Ren, Y. X. Fang and E. K. Wang, *ACS Nano*, 2011, **5**, 6425–6433.
24 M. Zhou, Y. Zhai and S. Dong, *Anal. Chem.*, 2009, **81**, 5603–5613.
25 Y. Du, S. J. Guo, H. X. Qin, S. J. Dong and E. K. Wang, *Chem. Commun.*, 2012, **48**, 799–801.
26 G. Zeng, Y. Xing, J. Gao, Z. Wang and X. Zhang, *Langmuir*, 2010, **26**, 15022–15026.
27 O. Leenaerts, B. Partoens and F. M. Peeters, *Phys. Rev. B: Condens. Matter Mater. Phys.*, 2009, **79**, 235440.
28 R. H. Zhou, G. H. Zuo, Q. Huang, G. H. Wei and H. P. Fang, *ACS Nano*, 2010, **4**, 7508–7514.
29 M. Calvaresi and F. Zerbetto, *ACS Nano*, 2010, **4**, 2283–2299.
30 X. Shi, A. von dem Bussche, R. H. Hurt, A. B. Kane and H. Gao, *Nat. Nanotechnol.*, 2011, **6**, 714–719.
31 J. Shi, H. Zhang, A. Snyder, M.-X. Wang, J. Xie, D. Marshall Porterfield and L. A. Stanciu, *Biosens. Bioelectron.*, 2012, **38**, 314–320.
32 J. Shen, Y. Hu, C. Li, C. Qin and M. Ye, *Small*, 2009, **5**, 82–85.
33 X. Xu, Q. Luo, W. Lv, Y. Dong, Y. Lin, Q. Yang, A. Shen, D. Pang, J. Hu, J. Qin and Z. Li, *Macromol. Chem. Phys.*, 2011, **212**, 768–773.
34 Z. Jin, T. P. McNicholas, C. J. Shih, Q. H. Wang, G. L. C. Paulus, A. Hilmer, S. Shimizu and M. S. Strano, *Chem. Mater.*, 2011, **23**, 3362–3370.
35 A. J. Patil, J. L. Vickery, T. B. Scott and S. Mann, *Adv. Mater.*, 2009, **21**, 3159–3164.
36 S. Zhang, Y. Shao, H. Liao, M. H. Engelhard, G. Yin and Y. Lin, *ACS Nano*, 2011, **5**, 1785–1791.
37 C. M. Wang, K. P. Liu, J. J. Zhang, G. H. Yang and J. J. Zhu, *Electrochem. Commun.*, 2010, **12**, 402–405.
38 Q. Zhang, Y. Qiao, F. Hao, L. Zhang, S. Wu, Y. Li, J. Li and X.-M. Song, *Chem.–Eur. J.*, 2010, **16**, 8133–8139.
39 L. Niu, C. S. Shan, H. F. Yang, J. F. Song, D. X. Han and A. Ivaska, *Anal. Chem.*, 2009, **81**, 2378–2382.

40 Q. Zeng, J. Cheng, L. Tang, X. Liu, Y. Liu, J. Li and J. Jiang, *Adv. Funct. Mater.*, 2010, **20**, 3366–3372.
41 T. S. Sreeprasad, M. S. Maliyekkal, K. Deepti, K. Chaudhari, P. L. Xavier and T. Pradeep, *ACS Appl. Mater. Interfaces*, 2011, **3**, 2643–2654.
42 P. Sutter, J. T. Sadowski and E. A. Sutter, *J. Am. Chem. Soc.*, 2010, **132**, 8175–8179.
43 C. Backes, F. Hauke and A. Hirsch, *Adv. Mater.*, 2011, **23**, 2588–2601.
44 S. Bose, T. Kuila, A. K. Mishra, N. H. Kim and J. H. Lee, *Nanotechnology*, 2011, **22**, 405603.
45 Y. Xu, H. Bai, G. Lu, C. Li and G. Shi, *J. Am. Chem. Soc.*, 2008, **130**, 5856–5857.
46 N. V. Kozhemyakina, J. M. Englert, G. A. Yang, E. Spiecker, C. D. Schmidt, F. Hauke and A. Hirsch, *Adv. Mater.*, 2010, **22**, 5483–5487.
47 S. M. Kozlov, F. Viñes and A. Görling, *Carbon*, 2012, **50**, 2482–2492.
48 J. Y. Shin, T. Premkumar and K. E. Geckeler, *Chem.–Eur. J.*, 2008, **14**, 6044–6048.
49 C. X. Guo, S. R. Ng, S. Y. Khoo, X. Zheng, P. Chen and C. M. Li, *ACS Nano*, 2012, **6**, 6944–6951.
50 J. Shi, T.-G. Cha, J. C. Claussen, A. R. Diggs, J. H. Choi and D. M. Porterfield, *Analyst*, 2011, **136**, 4916–4924.
51 C.-H. Lu, H.-H. Yang, C.-L. Zhu, X. Chen and G.-N. Chen, *Angew. Chem., Int. Ed.*, 2009, **48**, 4785–4787.
52 S. He, B. Song, D. Li, C. Zhu, W. Qi, Y. Wen, L. Wang, S. Song, H. Fang and C. Fan, *Adv. Funct. Mater.*, 2010, **20**, 453–459.
53 C. R. Edwards, W. Dang and S. L. Berger, *Biochemistry*, 2011, **50**, 10473–10483.
54 N. K. Sundlass and R. T. Raines, *Biochemistry*, 2011, **50**, 10293–10299.
55 C. Shan, H. Yang, D. Han, Q. Zhang, A. Ivaska and L. Niu, *Langmuir*, 2009, **25**, 12030–12033.
56 S. Some, S.-M. Ho, P. Dua, E. Hwang, Y. H. Shin, H. Yoo, J.-S. Kang, D.-k. Lee and H. Lee, *ACS Nano*, 2012, **6**, 7151–7161.
57 W. S. Hummers and R. E. Offeman, *J. Am. Chem. Soc.*, 1958, **80**, 1339.
58 W. Gao, L. B. Alemany, L. J. Ci and P. M. Ajayan, *Nat. Chem.*, 2009, **1**, 403–408.
59 D. Li, M. B. Muller, S. Gilje, R. B. Kaner and G. G. Wallace, *Nat. Nanotechnol.*, 2008, **3**, 101–105.
60 P.-C. Ma, N. A. Siddiqui, E. Mäder and J.-K. Kim, *Compos. Sci. Technol.*, 2011, **71**, 1644–1651.
61 J. C. Meyer, A. K. Geim, M. I. Katsnelson, K. S. Novoselov, T. J. Booth and S. Roth, *Nature*, 2007, **446**, 60–63.
62 J. Hermans, *J. Phys. Chem.*, 1966, **70**, 510–515.
63 B. B. Sauer, W. G. Kampert, R. S. McLean and R. Monteiro, *J. Polym. Sci., Part B: Polym. Phys.*, 2011, **49**, 222–243.
64 Y.-T. Shieh and G.-L. Liu, *J. Polym. Sci., Part B: Polym. Phys.*, 2007, **45**, 1870–1881.
65 G. V. Gurskaya, *Structure of Amino Acids [in Russian]*, Nauka, Moscow, 1966.
66 O. C. Compton, D. A. Dikin, K. W. Putz, L. C. Brinson and S. T. Nguyen, *Adv. Mater.*, 2010, **22**, 892–896.
67 A. Eckmann, A. Felten, A. Mishchenko, L. Britnell, R. Krupke, K. S. Novoselov and C. Casiraghi, *Nano Lett.*, 2012, **12**, 3925–3930.
68 A. Das, S. Pisana, B. Chakraborty, S. Piscanec, S. K. Saha, U. V. Waghmare, K. S. Novoselov, H. R. Krishnamurthy, A. K. Geim, A. C. Ferrari and A. K. Sood, *Nat. Nanotechnol.*, 2008, **3**, 210–215.
69 K. N. Kudin, B. Ozbas, H. C. Schniepp, R. K. Prud'homme, I. A. Aksay and R. Car, *Nano Lett.*, 2008, **8**, 36–41.
70 L. W. Chen and D. Wang, *Nano Lett.*, 2007, **7**, 1480–1484.
71 J. C. Ma and D. A. Dougherty, *Chem. Rev.*, 1997, **97**, 1303–1324.
72 S. Y. Jeong, S. H. Kim, J. T. Han, H. J. Jeong, S. Y. Jeong and G.-W. Lee, *Adv. Funct. Mater.*, 2012, **22**, 3307–3314.
73 Y. L. Wang and Y. C. Chang, *Macromolecules*, 2003, **36**, 6503–6510.
74 D. G. Dearborn and D. B. Wetlaufer, *Biochem. Biophys. Res. Commun.*, 1970, **39**, 314–320.
75 R. Yue, Q. Lu and Y. K. Zhou, *Biosens. Bioelectron.*, 2011, **26**, 4436–4441.
76 Z. H. Zhu, L. N. Qu, Q. J. Niu, Y. Zeng, W. Sun and X. T. Huang, *Biosens. Bioelectron.*, 2011, **26**, 2119–2124.
77 E. Laviron, *J. Electroanal. Chem.*, 1979, **100**, 263–270.
78 G. Y. Shi, Z. Y. Sun, M. C. Liu, L. Zhang, Y. Liu, Y. H. Qu and L. T. Jin, *Anal. Chem.*, 2007, **79**, 3581–3588.
79 A. Safavi, N. Maleki, O. Moradlou and M. Sorouri, *Electrochem. Commun.*, 2008, **10**, 420–423.